Direct analyses of fluorine in aqueous fluids extracted from 1-GPa experiments

Jia Wu, Kenneth T. Koga

Direct analyses of fluorine in aqueous fluids extracted from 1-GPa experiments

Jia Wu[1,*] and Kenneth T. Koga[2]

[1] State Key Laboratory of Petroleum Resources and Prospecting − College of Geoscience, China University of Petroleum, 102249, Beijing, China (jia.wu@cup.edu.cn)

[2] Laboratoire Magmas et Volcans, Université Clermont Auvergne, CNRS – UMR 6524, 6 Avenue Blaise Pascal, TSA 60026, 63178 AUBIERE Cedex, France

Declarations of interest: none

Abstract:

Fluorine has been proposed as a useful geochemical tracer for tracking the transport of volatile elements in subduction zones as it is the last volatile element to be exsolved during magma ascent and crystallization. Accurate determination of the concentration of fluorine in geological fluids under high *P-T* conditions would greatly further the understanding of its geochemical behavior during aqueous transport and magma genesis in arcs. Mass balance is the most widely used method for calculating fluid compositions in hydrothermal experiments. However, the method is inaccurate for large uncertainties of phase compositions and/or proportions. In the current study, we present an alternative method by directly measuring the concentration of F in fluids by extracting the enclosed liquid within experimental samples, and by performing high-pressure liquid chromatography (HPLC) measurement. We then compared the results of this direct analysis with those obtained by mass-balance calculations. Our experimental data demonstrate that direct analysis yields more accurate concentration values than mass-balance calculation. The direct method is a useful alternative, when i) the phase assemblage is complex, ii) the total F content or

the fluid proportion is low, or iii) when there is significant presence of hydrous melts. Caution should be exercised when applying direct analysis to samples that contained insoluble quench phases and/or were low in fluid. Direct HPLC analysis, combined with an improved extraction method that ensures the separation of quench phase, minerals and melts, could be of great utility for studying water-rock reactions.

Key words: fluorine; high $P-T$ experiments; aqueous fluid; HPLC

1. Introduction

Primitive melt inclusions are formed by the sequestration of primary lava inside crystallizing minerals during magma ascension. The main volatile species in these melt inclusions, which generally include H_2O, CO_2, S, Cl and F, are subjected to varying degrees of degassing as a result of magmatic ascent. Such partially–degassed magmas tend to retain initial abundance of F and Cl, while H_2O, CO_2, and SO_2 are significantly depleted (e.g., Villemant and Boudon, 1999). As these volatile elements are exclusively derived from subducting slabs, the retained halogens serve as ideal tracers for investigating the physico-chemical state and the mobility of volatile elements in subduction zones (Le Voyer et al., 2010; Spilliaert et al., 2006; Straub and Layne, 2003; Van den Bleeken and Koga, 2015; Wu and Koga, 2013). Data on the mineral-melt-fluid partitioning of F and Cl are therefore critical for geologists to deduce the conditions of magma genesis and the nature of slab flux. Although a number of research groups have measured the mineral-melt partition coefficients of F and/or Cl under high *P-T* conditions (Adam et al., 2016; Bernini et al., 2013; Beyer et al., 2012; Dalou et al., 2012; Dalou et al., 2014; Fabbrizio et al., 2013; Hauri et al., 2006; Joachim et al., 2015; O'Leary et al., 2010; Rosenthal et al., 2015; Van den Bleeken and Koga, 2015; Wu and Koga, 2013), there are significantly fewer studies on the distribution of these elements between aqueous fluids and mineral phases. This disparity is likely attributed to the difficulty in experimentally simulating water-rock reactions and accurately determining the chemical composition of fluid equilibrated under high *P-T* laboratory settings. Accurate quantification of the abundances of F and Cl in aqueous fluids is necessary for experimentally determining their fluid-mineral partition coefficients, which can provide key information on arc magmatism.

Mass balance is the most commonly used method for quantifying F and Cl in unquenchable aqueous fluids (i.e. fluids that undergo compositional changes during rapid cooling to ambient *P-T* conditions). The method assumes a closed system and attributes the mass difference between the bulk and the sum of all solid phases to the

fluid (Ayers et al., 1997; Bernini et al., 2013; Brenan et al., 1995; Chevychelov et al., 2008). To measure the mass fractions of F and Cl in minerals, a secondary ion mass spectrometer (SIMS) is used to analyze crystal grains with cross sections greater than 50 μm to ensure sufficient accuracy of measurement. Although mineral seeds are often used to promote crystal growth (Brenan et al., 1995) , they can partially dissolve in aqueous fluid under high *P-T* conditions, which changes the bulk composition and thus introduces uncertainties to mass-balance calculation. Also, the accuracy of mass balance decreases rapidly as the fluid fraction decreases (Koga et al., 2005). These drawbacks highlight the need for the development of an analytical methods that can directly determine fluid compositions.

High-pressure liquid chromatography (HPLC) has been used in a number of high *P-T* geological studies to determine the abundance of various fluid-soluble elements, including halogens, in aqueous systems. For example, Michel and Villemant (2003) quantified F and Cl in 17 reference rocks using digestion and HPLC. A similar strategy was employed to measure the concentrations of ammonium and potassium ions in fluid samples extracted from hydrothermal experiments (e.g. Pöter et al., 2004). In this study, we determined the F contents in aqueous solutions extracted from piston-cylinder hydrothermal experiments, which equilibrated with hornblende and a humite group mineral, using both direct HPLC analyses and mass-balance calculation. We also estimated the level of F in complex with cations such as Al, Fe and Mg in the extracted solution.

2. Experimental methods

2.1 Starting materials

Experiments were conducted with a natural mineral specimen composed mainly of Na_2O-FeO-CaO-MgO-Al_2O_3-SiO_2 with minor amounts of TiO_2, Cr_2O_3, and MnO. A total of four solid samples, designated SP1, SP2, SP3, and SP4, were prepared. SP1 - SP3 consisted of orthopyroxene (opx), clinopyroxene (cpx) and Al_2O_3 powder in

ratios that were slightly different but all stoichiometrically equivalent to that in hornblende (Hbl). SP4 was composed of SP1, SP3 and MgO. Both opx and cpx were handpicked from a coarse granular garnet lherzolite xenolith from Pali Aike, Chile (Stern et al., 1986). SP1 − SP4 were then doped with MgF_2 to the equivalent of 0, 5, 2 and 0.5 wt% F, respectively (Wu and Koga, 2013). The exact chemical composition of each sample was determined after converting it to homogeneous glass through annealing in graphite capsules at 1550 ºC and 1 GPa (Table 1). The bulk composition of SP4 was determined by mixing it with $LiBO_2$ (7.28 mg SP4 : 3.80 mg $LiBO_2$) to lower its melting point. As a consequence, the relative uncertainty of the composition of SP4 was greater than those of SP1 − SP3. The samples were individually weighed and loaded into separate capsules. Each capsule was weighed, followed by the addition of Milli-Q water with a micropipette. The capsules were weighed again after water loading. The seed-bearing experiment was performed with SP3 as starting material. Richterite crystals (amphibolite from the Western Alps) between 100 and 200 μm in width were added as seeds (Table 1).

2.2 Experiments

High $P-T$ experiments were conducted at Laboratoire Magmas et Volcans (LMV), Clermont-Ferrand, France, using piston-cylinder apparatuses that were 3/4 or 1/2 inch in diameter. The capsule was designed based on the cold-sealing technique described in Ayers et al. (1992) with minor modifications. The capsule size was reduced in order to minimize temperature gradients and to accelerate thermal equilibration. The outer chamber was manufactured with nickel, titanium or molybdenum, with dimensions as follows: outer diameter (od) = 4.0 (unit: mm, hereinafter), height (h) = 4.0, and a 3.2 long (l) central hole with a 2.1 or 3.1 inner diameter (id). The inner sleeves are gold or Au-Pd alloy tubes (od=2.0 or 3.0, thickness = 0.2, l = 5.0). The frictional pressure loss and temperature gradient associated with the standard assembly were corrected according to Laporte et al. (2004). Temperature was measured and controlled by a W_5Re_{95}-$W_{26}Re_{74}$ thermocouple. An 0.5 mm-thick aluminum disk was placed between the thermocouple

and the capsule to protect the former from contamination.

The experimental procedures were described in detail in Wu and Koga (2013). Briefly, the solid sample and Milli-Q water were loaded into the capsule, which was then placed in the piston cylinder. The pressure, temperature and experiment time were set to 1 GPa, 750 - 1057 ºC, and 34 - 215 h, respectively (Table 2). After quenching, the capsule was retrieved from the piston cylinder, cleaned of any adhering magnesium oxide, washed in an ultrasonic bath, and pierced with a blade. The punctured capsule was submerged in a beaker containing Milli-Q water and sonicated to extract the fluids within. This procedure was repeated two to four times to ensure the complete extraction of all soluble materials. The extraction solution from each sample was pooled in a volumetric flask and diluted 2,100 to 54,300 fold. The capsule was then oven-dried for one day at 120 ºC and weighed. The difference in the weight of the capsule before opening and after drying represented the combined mass of the fluid and the solid materials that were soluble in the extraction solution under ambient *P*-*T* conditions.

Because the formation of quench phases at higher pressure could affect the accuracy of mass-balance calculations, we also performed feasibility studies at 2.0 - 2.5 GPa and 877 ºC.

2.3 Determination of fluid composition

The fluid composition in each sample was determined by mass balance. The underlying assumption is that the total mass of an element in the bulk should be the sum of its masses in all phases. This can be expressed by the general equation shown below:

$$x_{Flu}^{i} = \frac{100 \cdot x_{bulk}^{i} - \sum_{s=1}^{n} (x_{s}^{i} \cdot \varphi_{s})}{\varphi_{Flu}} \quad (1)$$

where x_{bulk}^{i} and x_{s}^{i} represent the mass fractions of oxide *i* in the bulk and in phase *s*, respectively. φ_{s} and φ_{Flu} denote the proportion of phase *s* and fluid in the bulk, respectively. Because the system is assumed to have no mass exchange with the environment, the proportion of the bulk is set to 100%.

To determine the composition of a solid phase, the concentrations of major oxide species were measured by an electron probe microanalyzer (EMPA, CAMECA SX 100 at LMV). It is worth mentioning that we chose to measure F with a TAP detector to avoid potential interference with the tail L_{α}-line of Fe (e.g., Moune et al., 2007). Meanwhile, the mass fractions of water in hydrous minerals and hydrous melts were determined by stoichiometry and charge balance, respectively. To calculate the charge balance in hydrous melts, Fe was assumed to exist exclusively as Fe^{2+} (FeO). With the estimated mass fractions of water in hydrous minerals and melts, normalization was performed and the mass fractions of other elements in these phases were obtained, which were then applied to Equation (1). Detailed description of the mass-balance and charge-balance calculations used in this study can be found in Wu and Koga (2013) (section 2.5).

The extracted fluids, without further treatment, were analyzed on a DIONEX DX-120 Ion Chromatograph System at the Institute de Physique du Globe de Paris, France. Free fluoride (F^-) was measured by loading 1 mL of the fluid onto an AS9-HC column and eluting with 9 mmol/L Na_2CO_3 at a flow rate of 0.85 mL/min (Michel and Villemant, 2003). Calibration was performed every four runs by injecting a standard solution of 50 ppb F. All measurements were performed in duplicate. Detection limit was approximately 1 ppb, well below the lowest concentration of fluoride in the extracted solution (6 ppb). At this level, satisfactory reproducibility was still achieved between the duplicate measurements. Other F species, such as various F complexes, could not be detected by the column, which might lower the measurement accuracy by causing the total F content to be underestimated.

The quantitation of common cations such as Na^+, Mg^{2+}, Ca^{2+} and K^+ was performed following a similar protocol as described above with the following modifications. The fluid sample was loaded onto a CS12A column (Thermo Scientific^{TM}) and separation was performed by running 20 mmol/L CH_4O_3S as mobile phase at a flow rate of 0.98 mL/min.

ICP−MS measurement was conducted at Geosciences Environnement Toulouse. Each extraction solution was pre-mixed with 7-10 g of 5% in volume nitric acid and

0.12 g of an internal In/Re standard solution. Calibration was performed using three multi-element standards containing 1, 30 and 60 ppb of Mg, Ca, Al, Si, or Fe.

3. Results

Four different F-bearing samples, designated as SP1 (F-free), SP2 (F-rich), SP3 (intermediate-F), and SP4 (low-F), were tested under high $P-T$ conditions designed to simulate natural Hbl-bearing systems. The melt-free phase assemblage for each sample at 1 GPa was as follows: SP1 − Hbl; SP2 − Hbl and norbergite (Nrb, $Mg_2SiO_4{\cdot}Mg(OH)_2$); SP3 − Hbl and chondrodite (Chn, $Mg_2SiO_4{\cdot}2Mg(OH)_2$); SP4 − augite (Aug), clinohumite (Chu, $Mg_2SiO_4{\cdot}4Mg(OH)_2$), and Hbl or clintonite ($Ca_2(Mg,Al)_6(Si,Al)_8O_{20}(OH,F)_4$) (Table 2). The mineral species of the humite group in SP2 changed from Nrb to Chn, then to humite (Hu, $Mg_2SiO_4{\cdot}3Mg(OH)_2$) with increasing temperature. Specifically, the disappearance of Nrb in SP2 was observed at 947 ºC, whereas the formation of Chn and of Hu occurred at 977 ºC and 1057 ºC, respectively. In addition, hydrous melt in SP2 appeared at 947 ºC and its proportion steadily increased with rising temperature. In comparison, no Hbl was observed in SP2 at 2.5 GPa; instead, the phase assemblage of the sample consisted of hydrogrossular (OH-Grs, a hydrous garnet, with a chemical formula of $(Mg,Ca^{+})_3\,Al_2(SiO_4)_{3-x}(F,OH)_{4x}$), Nrb, Aug (Fig. 1a) and quench phase (Fig. 1b).

Back-scattered electron imaging indicated that large crystals were concentrated in the top section of the capsule (Fig. 2a). To obtain larger crystals, we increased the experimental time or temperature. However, running longer experiments at the same temperature resulted in greater water loss without notable improvement in crystal size (e.g., 1-SP2-24, which lasted 215 hours at 750 ºC). On the other hand, while we successfully generated larger crystals at higher temperatures, we also observed the formation of hydrous melts, which, for instance, occurred above 947 ºC in SP2 experiments. The melts contained 6.5 to 10.3 wt% of water based on the calculation of charge balance, and could be easily recognized by their vesicular texture that

resulted from fluid degassing and exsolution (Fig. 2c). Similar levels of water content have been reported by Holtz et al. (1995) in SiO_2-$NaAlSi_3O_8$-$KAlSi_3O_8$ systems at 0.5-8 kbar and 800 °C. Our results was also consistent with Mitchell et al. (2017)'s finding of a water solubility of 20.6 ± 0.9 wt% in basalt melt at 1 GPa and 1200 °C, as the water content of melt generally decreases with a drop in temperature.

We further investigated whether seeding could improve the crystal size. In 1-SP3-10, we seeded F-bearing Hbl with 10 μm-wide F-free Hbl grains derived from 1-SP1-8 (Fig. 2b). The similarity between the chemical composition of SP1 and that of SP3 could minimize the possibility of contamination introduced by seeding. Nevertheless, the seeds failed to induce the formation of sufficiently large Hbl crystals, suggesting that they either had dissolved or were too small. To address this problem, natural richterite seeds with width over 100 μm were used in 1-SP3-11. As illustrated in Fig. 2d, back-scattered electron imaging revealed the formation of a smooth boundary around the seed crystal, suggesting its partial dissolution prior to the precipitation of new crystals. EMPA showed that the overgrowth comprised two zones with slightly different compositions (Fig. 2d). Specifically, the contents of MgO and SiO_2 in Zone 1 were shown to be greater than those in Zone 2 by 1 wt% and 4 wt%, respectively. On the other hand, the levels of CaO, Al_2O_3 and F in Zone 1 were 1 wt%, 6 wt% and 0.1 wt% lower than their respective counterparts in Zone 2. These results highlighted the potential impact that seeding might produce on the bulk composition and those of the newly precipitated crystals.

4. Discussion

4.1 Limitations and validation of the mass-balance approach

One of the most significant contributing factors to inaccurate mass balance results is the unintended loss of materials by diffusion and/or leakage, as well as the inadvertent introduction of contaminants. Such anomalies have been reported in a number of studies. Ayers et al. (1997) observed that hydrogen generated from the

thermal decomposition of water could diffuse through gold capsule and contribute to the decrease of aqueous fluids. In one of Brenan and Watson (1991)'s experiments, fluid expansion during quenching was suspected to have caused capsule failure and vapor leakage. Absorption of Fe by Pt-based capsules was noted by Watson (1991). This loss could not be completely prevented even by pre-saturating the capsule with Fe-bearing compounds (personal communication with C. Dalou). Based on these findings, we identified four factors that could compromise the accuracy of mass-balance calculations in our current study.

First, loss of materials was suspected in some experiments of this study, such as in 1-SP2-14, which had a considerably different phase assemblage (Hbl-Nrb-Chn-Flu) from other SP2 runs (Hbl-Nrb-Flu). The observation of Chn, which contains less F than Nrb, suggested a decreased abundance of the halogen in the bulk of 1-SP2-14. Because missing mass had to be assumed as part of the fluid, this anomaly in bulk composition artificially inflated the calculated level of F in the fluid. Similarly, in 1-SP2-23, sonication of the capsule might have led to an inadvertent loss of spinel crystals rich in Al, Mg and Fe, causing the mass-balance method to overestimate the concentration of Al in the fluid. In some cases, low-abundance solid phases could elude detection and thus not be included in the mass-balance calculations. When we compared the data of different SP3 experiments, we noticed that a small proportion of Chn (<6 wt%) was observed in all runs except 1-SP3-1, 10 and 11. Further investigation revealed that the composition of Hbl remained almost constant in these experiments, but the fluid proportion varied significantly. Taken together, these results implied that all SP3 experiments should have reached phase equilibrium at the end, which in turn suggested that the absence of Chn in 1-SP3-1, 10 and 11 was likely due to detection errors. Therefore, in subsequent mass-balance calculations, we corrected the phase assemblage of 1-SP3-1 by assuming that its composition of Chn was identical to that in 1-SP3-3, based on the fact that both runs used the same starting sample and were conducted under similar *P*-*T* conditions.

Second, when determining the chemical composition of a solid phase, the results obtained from the measurement of a few large crystals are often not sufficiently

representative due to phase inhomogeneity. A previous study described by Larocque and Canil (2010) showed that the abundances of Al and Si in hornblende varied significantly according to the pressure and temperature at which the phase was formed. Based on this finding, we speculated that the comparatively large uncertainties of the mass fractions of Si and Al in hornblende that we observed in our experiments could also have been caused by the temperature gradient in the lower capsule.

Third, the calculation of phase proportions, which are an essential part of the mass-balance equation, involves the selection of conservative elements and the determination of their concentrations. Although the mass-balance method assumes these elements to be completely insoluble, this is generally not true under high *P-T* conditions. In fact, mass balance likely produced incorrect phase proportion results in many experiments that involved SP4 or hydrous melts (Table 2), as the calculation of F content in the fluid yielded zero or negative values in obvious contradiction to direct HPLC analysis. One emerging strategy that could potentially improve the accuracy in the measurement of phase proportion is to directly visualize and quantify mineral distribution by computed tomography (CT) imaging (Friese et al., 2013). It is worth emphasizing that non-metal capsules or sample removal from metal capsules would be required.

Fourth, the accuracy of mass balance decreases as the proportion of fluid in the sample drops. Koga et al. (2005) argued that having more mineral-compatible elements and less fluids in fluid-bearing experiments would increase the uncertainties of the fluid compositions and partition coefficients via mass-balance approach. In the current study, as F resided mostly in hydrous minerals, decreased fluid proportion in samples would reduce the accuracy of the mass-balance method (Fig. 3). Based on our estimates, the relative uncertainty of F abundance in fluid calculated by mass balance could exceed 100% when its proportion drops below 50 wt%, which is consistent with Koga et al. [2005]'s modeling of error propagation in mass-balance calculations. This would ultimately generate large uncertainties in partition coefficients between fluids and minerals, which can only bring a weak constraint on the geochemical behavior of tracer elements.

One way to validate the mass-balance approach is to compare the abundances of Si, Al, Mg and Ca in the extracted fluids calculated by mass balance to their literature values. The normal SiO_2 concentrations in the fluids by mass-balance calculations were in the range of 1.09-5.61 wt%, which was in good agreement with Newton and Manning (2002)'s study (2.9 wt% SiO_2, equilibrium with enstatite-forsterite-H_2O systems at 1 GPa and 700-900 °C). However, several experiments, such as in 1-SP2-23 (11.86 wt%) and 1-SP3-3 (18.82 wt%), exhibited abnormally high levels of SiO_2, presumably due to water loss and/or other compositional changes that invalidated the closed-system assumption. Meanwhile, the concentrations of Al_2O_3 in the aqueous fluid ranged from 0.26 to 1.77 wt%, echoing Manning et al.'s finding that Al is less soluble than Si in the assemblage of albite-paragonite-quartz at 1 GPa and 350-620 ºC (Manning et al., 2010). Moreover, our ICP-MS data also indicated that SiO_2 (0.27-7.86 wt%) was more abundant in the fluid than Al_2O_3 (0.009-0.37 wt%) in Hbl-Hu systems. In addition, mass-balance calculations and ICP-MS quantitation found very low levels of MgO (0.016-0.25 wt%) and CaO (0.028-0.373 wt%) in the fluids. Taken together, we conclude that mass-balance results in most of our experiments are consistent with those reported previously. Despite the limitations described above, we argue that mass balance should be particularly useful in experiments with a relatively simple phase assemblage (e.g. certain SP2 and SP3 experiments that involved only two to three mineral phases).

4.2 Quantitation of soluble elements F and Na in fluids

We measured the concentration of F in the fluid via both mass balance and direct analysis. As shown in Fig. 4a, the two approaches were largely consistent with each other in most 1-GPa SP2 and SP3 experiments. On the one hand, the mass-balance method showed that the levels of F in the fluids extracted from SP2 and SP3 runs were 0.2-0.8 wt% and 0.06-0.4 wt%, respectively, with uncertainties in the range of 0.16 wt% to 2.6 wt% or relative uncertainties of 57% to 370%. In comparison, HPLC quantitation showed that the level of aqueous F ranged between 0.057 wt% and 0.56 wt% in SP2 runs, and between 0.029 wt% and 0.106 wt% in SP3, with substantially

smaller uncertainties (0.001-0.01 wt%) than those of the mass-balance method. On the other hand, the levels of F calculated by mass balance greatly exceeded those of direct HPLC analysis in all 2- and 2.5-GPa experiments (2 GPa: mass balance – 1.65 wt%, direct analysis – 0.365 wt%; 2.5 GPa: mass balance – 1.09 wt%, direct analysis – 0.055 wt%). This was likely due to the presence of F in the quench phase (Fig. 1b), which sequestered soluble elements, rendering them unextractable and thus inaccessible to HPLC analysis, and to the larger proportion of quench phase at higher pressures. System leakage could also cause mass-balance results to be significantly greater than those of direct analysis for the obvious reason that lost F-bearing materials were not extracted and therefore not measured. Finally, in 1-SP2-21, 1-SP4-3 & 4, 1-(SP2+Qtz) and 1-(SP1+MgF_2), mass-balance calculations yielded negative F concentrations, whereas HPLC quantitation was apparently not affected due to its low detection limit. Overall, HPLC results were shown to be reliable when the proportion of quench phase in the bulk was less than 10% in volume of total solid phases (estimated by cross-section image).

In comparison, mass balance and direct analysis generated comparable levels of Na (Fig. 4b). One obvious reason for the better consistency was that the solubility of Na in water is much higher than that of F, resulting in lower relative uncertainties. An additional contributing factor is that the quench phase usually contained disproportionate amounts of cations such as Si, Al, Mg and Ca, which could sequester F^- and other negatively charged F-bearing species via electrostatic interaction. Consequently, a significant portion of these F species could have been transferred from the fluid to the quench phase and became unextractable. Taken together, the results of mass balance and direct analysis are both acceptable in most experiments; however, there are scenarios in which one method would be more preferred than the other. Mass-balance calculations are prone to yield negative concentration values when the total F content in the bulk is low, whereas direct analysis is not suitable for samples that contain significant amounts of unextractable F-bearing quenched solutes.

4.3 Assessing the accuracy of direct HPLC analysis

The total fluorine in extracted fluid can exist as F^-, HF, and/or fluoride-based complexes such as SiF_6^{2-} and AlF_6^{3-}. However, only F^- can be quantified on the AS9-HC column used in the current study. Therefore, the exact chemical form of fluorine before and during HPLC analysis plays a crucial role in ensuring accurate measurement. Nevertheless, we reasoned that the strong alkalinity (pH ~ 12) of the mobile phase and the dilution of the recovered fluid should ensure the near-complete conversion of HF to F^-.

SiF_4 and its derivatives can also be found in various geological fluids and gases. For example, SiF_4 has been detected in volcanic plume via remote observation employing FT-IR spectroscopy (Mori et al., 2002). Although the presence of SiF_4 in high P–T fluid has not been reported, it is known to be able to form H_2SiF_6 and silica in aqueous solutions under ambient conditions (Aigueperse et al., 2000). Mirroring these findings, our previous mass-balance calculations revealed a positive correlation between the aqueous concentration of F and the solubility of Si, implying that the two elements might have reacted and formed soluble species, possibly SiF_6^{2-}, under the experimental conditions involved in the study (Wu and Koga, 2013). However, SiF_6^{2-} has been shown to completely hydrolyze at pH > 4 (Finney et al., 2006), which would lead to the release of F^- and its subsequent detection by HPLC. Therefore, SiF_6^{2-} was unlikely to be a major fluorine species in the fluid during the HPLC analysis.

The contribution of various metal-fluoride species to measurement uncertainties can be estimated by calculating the fractions of F in these complexes based on their association constants (Lange and Speight, 2005), the concentration of F^- determined by HPLC, and the total level of each metal measured from ICP-MS measurement (Table 3). Given that the relative uncertainty of the HPLC method is approximately 1%, we concluded that aluminum, iron and magnesium fluorides together accounted for less than 0.3% of total aqueous F and thus could be safely ignored. This also suggested that dilution of the extracted fluid also promoted the dissociation of the metal-fluoride species.

Taken together, the dissociation of various F-bearing complexes and the deprotonation of HF were strongly favored due to the chemical nature of the eluent.

Consequently, free F^- was by far the predominant form of fluorine during HPLC analysis and its concentration could be safely used to approximate that of total F in the fluid.

4.4 Limitation of the direct analysis method

The primary error source of the direct analysis method is the change of fluid composition during quenching and/or annealing. Rapid cooling of the capsule could result in the crystallization of quench phases and/or the exsolution of fluid from hydrous melts depending on the run conditions. In addition, water loss could lead to the saturation and subsequent precipitation of certain solutes from the fluid.

The precipitation of insoluble quench phases greatly affects the accuracy of direct analysis by trapping otherwise extractable elements such as Na and F. As discussed in Section 3.1, we argued that the mass-balance method could be suitable for estimating the aqueous concentration of F in 3-SP2-1 because the bulk was F-rich and contained only two solid phases, Hbl and Nrb. The discrepancy between mass balance and HPLC analysis (2 GPa: mass balance – 1.65 wt%, direct analysis – 0.365 wt%) was probably due to the significant amount of quench phases (e.g., Ayers et al., 1997). One strategy to re-solubilize the trapped elements is through the recovery of quench phases. For example, Koga et al. (2005) demonstrated that certain types of quench phase could be re-dissolved by washing with acidic or alkaline reagents, which would reduce their detrimental impact on direct analysis.

The exsolution of water from liquid-rich hydrous melts poses an additional problem by increasing the mass of the extractable fluid. Van den Bleeken and Koga (2015)'s study of water-enriched melts has shown F to be quenchable in silicic glasses, which echoed the general observation that F is least affected by degassing among all major volatiles (e.g., Spilliaert et al., 2006; Villemant and Boudon, 1999). We speculated that the formation of hydrous melts in 1-GPa experiments (>900 °C), as evidenced by their vesiculated texture, might cause the aqueous level of F to be underestimated (Fig. 2c). Therefore, it is strongly recommended to run the experiment at temperatures below the solidus.

The reliability of direct analysis could also vary according to the amount of fluid present in the sample. This effect was shown by plotting the fluid proportion against the aqueous F content determined by HPLC in each run. As illustrated in Fig. 5, the HPLC concentrations were relatively constant and in agreement with those obtained by mass-balance calculations (SP2: 0.30 ± 0.10 wt%; SP3: 0.15 ± 0.10 wt%) when the fluid proportions were above 30 wt%. In contrast, the levels of F in the fluid were apparently overestimated at low fluid proportions, particularly in SP2 experiments. One possible explanation is that the decreased amount of fluid in the sample could lead to incomplete convective mixing of liquid in different parts of the capsule, causing otherwise soluble F-bearing species to become locally saturated and precipitate. Such precipitates were often extractable under ambient conditions and would therefore artificially boost the aqueous level of F during HPLC analysis. This might also have occurred in studies using capsule with diamond trap technique (Stalder et al., 2001). Taken together, the precipitation of otherwise soluble F-bearing species in dehydrated samples would cause the level of F in fluid to be overestimated by both mass-balance calculations and direct analysis.

We thus screened our results and identified all experiments that were generally unaffected by the abovementioned detrimental factors. The $D_F^{Flu/Hbl}$ derived from HPLC measurements in these runs were highlighted in ***bold italic font*** in Table 2. Consistent with our previous study, $D_F^{Flu/Hbl}$ from SP2 and SP3 experiments is independent of temperature. Thus, we used the weighted average of $D_F^{Flu/Hbl}$ in each group. The unpaired Student's t-test gives that t=8.6824, and the two-tailed P-value is less than 0.0001, which suggests to reject the null hypothesis. Thus, the weighted averages of the partition coefficients from HPLC concentrations were found to be significantly different between the qualified SP2 (0.042 ± 0.003) and SP3 (0.029 ± 0.002) experiments at the pressure of 1 GPa. In contrast, no such discrepancy was detected between the two groups based on a similar examination of the mass balance results using the same test (SP2: 0.14 ± 0.05; SP3: 0.10 ± 0.07). This suggested that the direct analysis method showed greater precision than mass balance and might be suitable for investigating the migration patterns of (volatile) elements in the

subduction zone.

5. Conclusions

The results of our study demonstrated the feasibility of using HPLC analysis to directly measure the concentration of F in aqueous fluids at 1 GPa and below solidus. The obtained HPLC data suggested that the mass-balance calculation results of soluble elements were generally reliable in 1-GPa experiments. Meanwhile, it should be noted that the direct analysis method showed considerable depletion of elements when the bulk contained a significant proportion of quench phase, e.g., experiments above 2 GPa.

Secondly, both mass balance and direct analysis were shown to have incorrectly included the exsolved content of hydrous melt and/or the precipitates from extracted fluids caused by local saturation. Therefore, a fluid/solid ratio above 0.4 is recommended for HPLC measurement of F or any other analyzable elements. It is also necessary to improve the current annealing method in order to promote fluid convection (or stirring), such as using rocking high-pressure apparatus (Schmidt and Ulmer, 2004).

Lastly, the HPLC method could also be employed to quantify other volatile species (e.g., halogens, sulfur, and NH_4^+) and soluble cations (e.g., Li^+) in aqueous fluids from high $P-T$ environments. Post-quench treatment might be necessary to recover quench phases from experimental capsules to improve the accuracy of HPLC analysis (e.g., Ayers et al., 2012; Koga et al., 2005).

Acknowledgements

We would like to thank Jean-Luc Devidal (LMV) for his help with the electron microprobe analysis and Agnès Michel, and Calorine Gorge (IPGP) for their help with the high pressure liquid chromatography analysis. We also acknowledge advice on

HPLC from Aurelie Colomb during the early stage of this study, and a mass-balance calculation suggestion for fluid composition from John Ayers. We appreciate Mhammed Benbakkar (LMV) for ICP-AES measurements, and Frederic Candaudap (Geosciences Environnement Toulouse) for ICP-MS analyses on our fluid samples. We also would like to thank Franck Pointud and Fabrice Doré for their work on the piston-cylinder apparatus, and Jean-Louis Fruquiere for disciplined machining on the piston-cylinder assemblages. Finally, we appreciate the editor Professor Donald Dingwell and the reviewer John Ayers, whose constructive suggestions greatly promoted the quality of this manuscript. This work was supported by National Natural Science Foundation of China (No. 41403049), ANR SlabFlux (ANR09BLAN0338) and the Foundation of State Key Laboratory of Petroleum Resources and Engineering, China University of Petroleum, Beijing (No. PRP/indep-3-1715). This is Laboratory of excellence *ClerVolc* contribution n° X.

References:

Adam, J., Turner, M., Hauri, E.H., Turner, S., 2016. Crystal/melt partitioning of water and other volatiles during the near-solidus melting of mantle peridotite: Comparisons with non-volatile incompatible elements and implications for the generation of intraplate magmatism. American Mineralogist, 101: 876-888.

Aigueperse, J. et al., 2000. Fluorine Compounds, Inorganic, Ullmann's Encyclopedia of Industrial Chemistry. Wiley-VCH Verlag GmbH & Co. KGaA.

Ayers, J.C., Brenan, J.M., Bruce Watson, E., Wark, D.A., Minarik, W.G., 1992. A new capsule technique for hydrothermal experiments using the piston-cylinder apparatus. American Mineralogist, 77(9-10): 1080-1086.

Ayers, J.C., Dittmer, S.K., Layne, G.D., 1997. Partitioning of elements between peridotite and H_2O at 2.0–3.0 GPa and 900–1100 °C, and application to models of subduction zone processes. Earth and Planetary Science Letters, 150(3–4): 381-398.

Ayers, J.C., Zhang, L., Luo, Y., Peters, T.J., 2012. Zircon solubility in alkaline aqueous fluids at upper crustal conditions. Geochimica Et Cosmochimica Acta, 96: 18-28.

Bernini, D., Wiedenbeck, M., Dolejs, D., Keppler, H., 2013. Partitioning of halogens between mantle minerals and aqueous fluids: implications for the fluid flow regime in subduction zones. Contributions to Mineralogy and Petrology, 165(1): 117-128.

Beyer, C., Klemme, S., Wiedenbeck, M., Stracke, A., Vollmer, C., 2012. Fluorine in nominally fluorine-free mantle minerals: Experimental partitioning of F between olivine, orthopyroxene and silicate melts with implications for magmatic processes. Earth and

Planetary Science Letters, 337: 1-9.

Brenan, J.M., Shaw, H.F., Ryerson, F.J., Phinney, D.L., 1995. Mineral-aqueous fluid partitioning of trace elements at 900 °C and 2.0 GPa: Constraints on the trace element chemistry of mantle and deep crustal fluids. Geochimica et Cosmochimica Acta, 59(16): 3331-3350.

Brenan, J.M., Watson, E.B., 1991. Partitioning of trace elements between olivine and aqueous fluids at high *P-T* conditions: implications for the effect of fluid composition on trace-element transport. Earth and Planetary Science Letters, 107(3–4): 672-688.

Chevychelov, V.Y., Botcharnikov, R.E., Hoitz, F., 2008. Partitioning of Cl and F between fluid and hydrous phonolitic melt of Mt. Vesuvius at similar to ~850–1000 °C and 200 MPa. Chemical Geology, 256(3-4): 172-184.

Dalou, C., Koga, K., Shimizu, N., Boulon, J., Devidal, J.-L., 2012. Experimental determination of F and Cl partitioning between lherzolite and basaltic melt. Contributions to Mineralogy and Petrology, 163(4): 591-609.

Dalou, C., Koga, K.T., Le Voyer, M., Shimizu, N., 2014. Contrasting partition behavior of F and Cl during hydrous mantle melting: implications for Cl/F signature in arc magmas. Progress in Earth and Planetary Science, 1(1): 1-17.

Fabbrizio, A., Stalder, R., Hametner, K., Gunther, D., 2013. Experimental chlorine partitioning between forsterite, enstatite and aqueous fluid at upper mantle conditions. Geochimica Et Cosmochimica Acta, 121: 684-700.

Finney, W.F., Wilson, E., Callender, A., Morris, M.D., Beck, L.W., 2006. Reexamination of Hexafluorosilicate Hydrolysis by 19F NMR and pH Measurement. Environmental Science & Technology, 40(8): 2572-2577.

Friese, K.I., Cichy, S.B., Wolter, F.E., Botcharnikov, R.E., 2013. Analysis of tomographic mineralogical data using YaDiV-Overview and practical case study. Computers & Geosciences, 56: 92-103.

Hauri, E.H., Gaetani, G.A., Green, T.H., 2006. Partitioning of water during melting of the Earth's upper mantle at H_2O-undersaturated conditions. Earth and Planetary Science Letters, 248(3-4): 715-734.

Holtz, F., Behrens, H., Dingwell, D.B., Johannes, W., 1995. H_2O solubility in haplogranitic melts: Compositional, pressure, and temperature dependence. American Mineralogist, 80(1-2): 94-108.

Joachim, B. et al., 2015. Experimental partitioning of F and Cl between olivine, orthopyroxene and silicate melt at Earth's mantle conditions. Chemical Geology, 416: 65-78.

Koga, K.T., Daniel, I., Reynard, B., 2005. Determination of trace element partition coefficients between water and minerals by high-pressure and high-temperature experiments: Leaching technique. Geochemistry Geophysics Geosystems, 6.

Lange, N.A., Speight, J.G., 2005. Lange's handbook of chemistry. McGraw-Hill standard handbooks. McGRAW-HILL, New York.

Laporte, D., Toplis, M., Seyler, M., Devidal, J.-L., 2004. A new experimental technique for extracting liquids from peridotite at very low degrees of melting: application to partial melting of depleted peridotite. Contributions to Mineralogy and Petrology, 146(4): 463-484.

Larocque, J., Canil, D., 2010. The role of amphibole in the evolution of arc magmas and crust: the case from the Jurassic Bonanza arc section, Vancouver Island, Canada.

Contributions to Mineralogy and Petrology, 159(4): 475-492.

Le Voyer, M., Rose-Koga, E.F., Shimizu, N., Grove, T.L., Schiano, P., 2010. Two Contrasting H_2O-rich Components in Primary Melt Inclusions from Mount Shasta. Journal of Petrology, 51(7): 1571-1595.

Manning, C.E., Antignano, A., Lin, H.A., 2010. Premelting polymerization of crustal and mantle fluids, as indicated by the solubility of albite+paragonite+quartz in H_2O at 1 GPa and 350–620 °C. Earth and Planetary Science Letters, 292(3–4): 325-336.

Michel, A., Villemant, B., 2003. Determination of halogens (F, Cl, Br, I), sulfur and water in seventeen geological reference materials. Geostandards Newsletter-the Journal of Geostandards and Geoanalysis, 27(2): 163-171.

Mitchell, A.L., Gaetani, G.A., O'Leary, J.A., Hauri, E.H., 2017. H_2O solubility in basalt at upper mantle conditions. Contributions to Mineralogy and Petrology, 172(10): 85.

Mori, T., Sato, M., Shimoike, Y., Notsu, K., 2002. High SiF_4/HF ratio detected in Satsuma-Iwojima volcano's plume by remote FT-IR observation. Earth Planets and Space, 54(3): 249-256.

Moune, S., Sigmarsson, O., Thordarson, T., Gauthier, P.J., 2007. Recent volatile evolution in the magmatic system of Hekla volcano, Iceland. Earth and Planetary Science Letters, 255(3-4): 373-389.

Newton, R.C., Manning, C.E., 2002. Solubility of enstatite + forsterite in H_2O at deep crust/upper mantle conditions: 4 to 15 kbar and 700 to 900 °C. Geochimica et Cosmochimica Acta, 66(23): 4165-4176.

O'Leary, J.A., Gaetani, G.A., Hauri, E.H., 2010. The effect of tetrahedral Al^{3+} on the partitioning of water between clinopyroxene and silicate melt. Earth and Planetary Science Letters, 297(1-2): 111-120.

Pöter, B., Gottschalk, M., Heinrich, W., 2004. Experimental determination of the ammonium partitioning among muscovite, K-feldspar, and aqueous chloride solutions. Lithos, 74(1–2): 67-90.

Rosenthal, A., Hauri, E.H., Hirschmann, M.M., 2015. Experimental determination of C, F, and H partitioning between mantle minerals and carbonated basalt, CO_2/Ba and CO_2/Nb systematics of partial melting, and the CO_2 contents of basaltic source regions. Earth and Planetary Science Letters, 412: 77-87.

Schmidt, M.W., Ulmer, P., 2004. A rocking multianvil: Elimination of chemical segregation in fluid-saturated high-pressure experiments. Geochimica et Cosmochimica Acta, 68(8): 1889-1899.

Spilliaert, N., Métrich, N., Allard, P., 2006. S–Cl–F degassing pattern of water-rich alkali basalt: Modelling and relationship with eruption styles on Mount Etna volcano. Earth and Planetary Science Letters, 248(3–4): 772-786.

Stalder, R., Ulmer, P., Thompson, A.B., Gunther, D., 2001. High pressure fluids in the system MgO-SiO_2-H_2O under upper mantle conditions. Contributions to Mineralogy and Petrology, 140(5): 607-618.

Stern, C.R., Saul, S., Skewes, M.A., Futa, K., 1986. Garnet peridotite xenoliths from the Pali-Aike alkali basalts of southernmost South America. In: Ross, J. (Editor), Fourth International Kimberlite Conference. Geological Society of Australia, Perth, Australia, pp. 735-744.

Straub, S.M., Layne, G.D., 2003. The systematics of chlorine, fluorine, and water in Izu arc front volcanic rocks: Implications for volatile recycling in subduction zones. Geochimica Et Cosmochimica Acta, 67(21): 4179-4203.

Van den Bleeken, G., Koga, K.T., 2015. Experimentally determined distribution of fluorine and chlorine upon hydrous slab melting, and implications for F-Cl cycling through subduction zones. Geochimica Et Cosmochimica Acta, 171: 353-373.

Villemant, B.t., Boudon, G., 1999. H_2O and halogen (F, Cl, Br) behaviour during shallow magma degassing processes. Earth and Planetary Science Letters, 168(3–4): 271-286.

Watson, E.B., 1991. Diffusion in fluid-bearing and slightly-melted rocks - experimental and numerical approaches illustrated by iron transport in dunite. Contributions to Mineralogy and Petrology, 107(4): 417-434.

Wu, J., Koga, K.T., 2013. Fluorine partitioning between hydrous minerals and aqueous fluid at 1 GPa and 770–947 °C: A new constraint on slab flux. Geochimica et Cosmochimica Acta, 119(0): 77-92.

Fig. 1 Back-scattered electron images of 4-SP2-1 experiment at 2.5 GPa and 877 ºC. The dark area surrounding minerals is pore space impregnated by epoxy. This open space indicates the presence of a large volume of fluid during annealing, which benefits large crystals growth. The scale bar at the bottom indicates 200 μm. a) Phase assemblies: hydrogrossular (Hgr), augite (Aug), and chondrodite (Chn). b) The quench phases, which are present next to the wall in the middle portion of the capsule, are too small (< 5 μm) to be analyzed by electron microprobe. The presence of significant quench phases reveals that the content of the extracted fluid is depleted in elements that are insoluble at ambient conditions.

Fig. 2 Back-scattered electron images for typical 1-GPa experiments. a) The middle portion of 1-SP3-4 experiment at 837 ºC. The scale bar is 500 μm. The elongated minerals are Hbl, and the two grey lumpish crystals in the center are Chd. The bright parts are gold chips. b) The bottom portion of 1-SP1-8 experiment at 807 ºC. The scale bar is 500 μm. Hbl is the unique mineral phase in this run. The crystals are all small and are distributed evenly in the bottom of the charge. c) Cross section texture of the hydrous melt in experiment 1-SP2-18. The grey holes in the center of the melt indicate the degassing and exsolution during quench. d) One big Hbl crystal grows with a seed in 1-SP3-11 experiment at 750 ºC. The lighter part is the seed crystal. Zone 1 and Zone 2 are both new overgrowths and differ slightly on the compositions. Zone 2 has more F than Zone 1.

Fig. 3 The standard deviation (2σ, wt%) of F concentration in aqueous fluids versus fluid proportion (wt%) after quench. All the data are based on 1-GPa experiments. Blue diamond, red square, and orange triangle symbols represent the starting materials of SP2 (5 wt% F), SP3 (1.9 wt% F), and SP4 (0.5 wt% F) respectively. In a general tendency, the standard deviation of F concentration from mass balance calculation (solid symbols) decreases with fluid proportion increasing in bulk composition. On the contrary, the standard deviation of F concentration from HPLC analyses (open symbols) is independent with fluid proportion, and is one magnitude order lower than those from mass balance result.

Fig. 4 The comparisons of a) F and b) Na_2O concentrations in fluids between HPLC and

mass balance calculation. Blue diamond, red square, orange triangle and blue crossing symbols represent the starting materials of SP2 (5 wt% F), SP3 (1.9 wt% F), SP4 (0.5 wt% F) and Mix composition, respectively. The experiments mentioned above were conducted at 1 GPa. Black open round represents the SP2 experiments under 2 GPa and 2.5 GPa. A black solid line y=x was plotted as a reference.

Fig. 5 F concentrations of aqueous fluids measured by HPLC versus fluid proportion (wt%) in bulk composition after quenching. The data setting is the same with Fig. 3. Each solid line and dashed line of the same color represents the average level of F determined by mass balance and the uncertainty, respectively, in the corresponding experiment run. The corresponding experimental temperature is attached below (blue) and above (red) the symbols of SP2 and SP3 experiments, respectively. F concentration decreases dramatically when fluid proportion increases from 20 to 40 wt%, and then almost constant when fluid proportion is larger than 30 wt%.

Figure 1a

Click here to download high resolution image

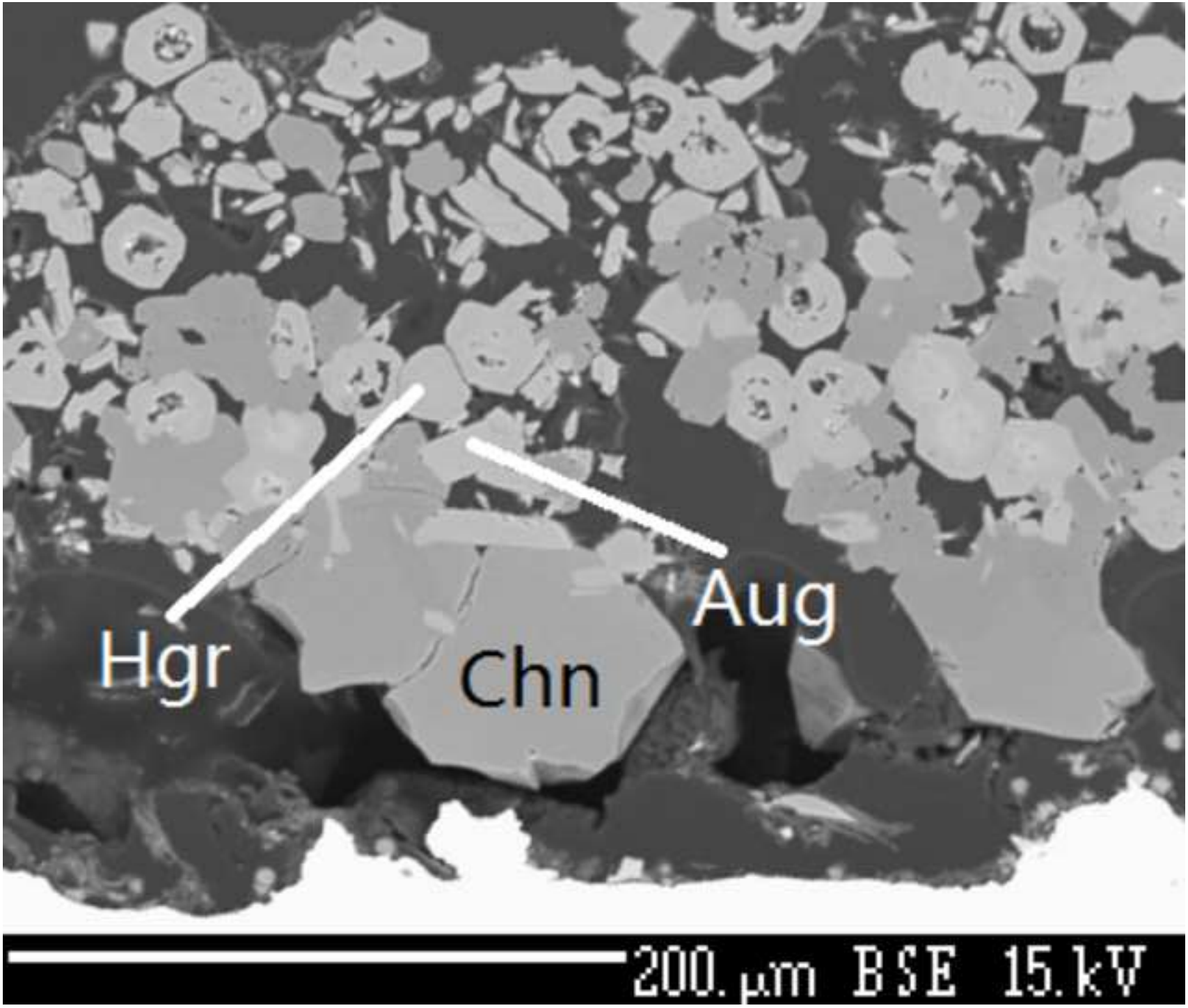

Figure 1b

Click here to download high resolution image

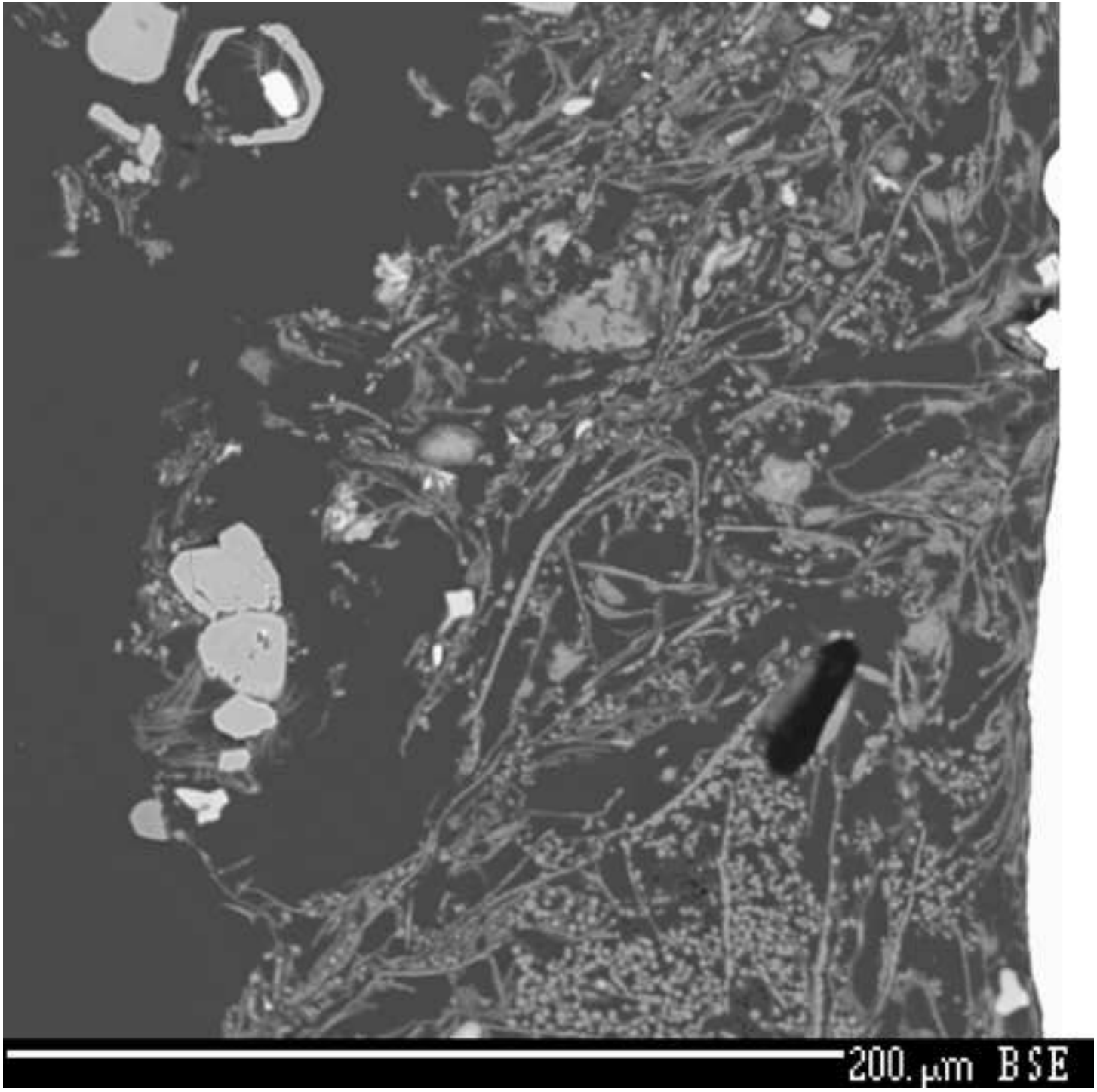

Figure 2a

Click here to download high resolution image

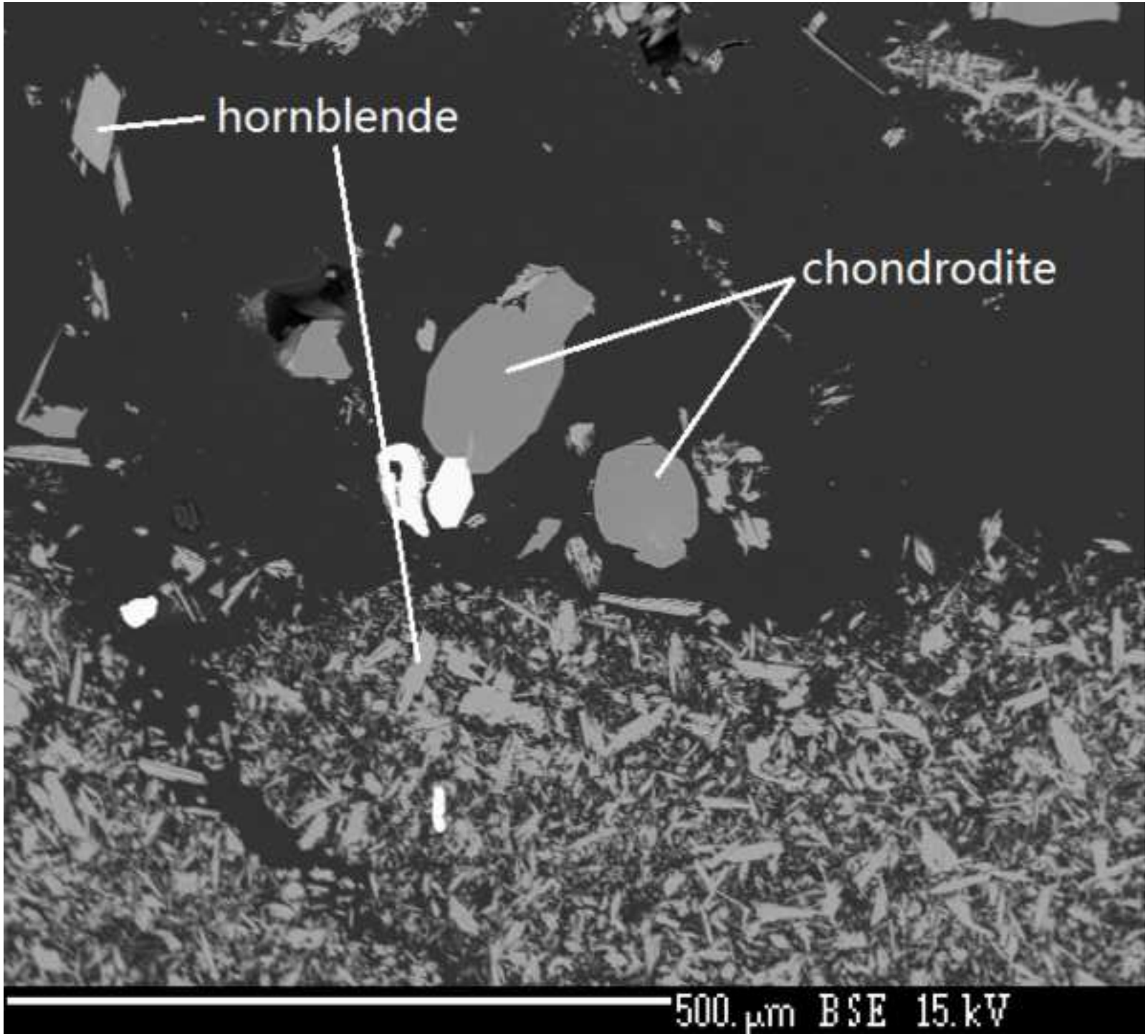

Figure 2b

Click here to download high resolution image

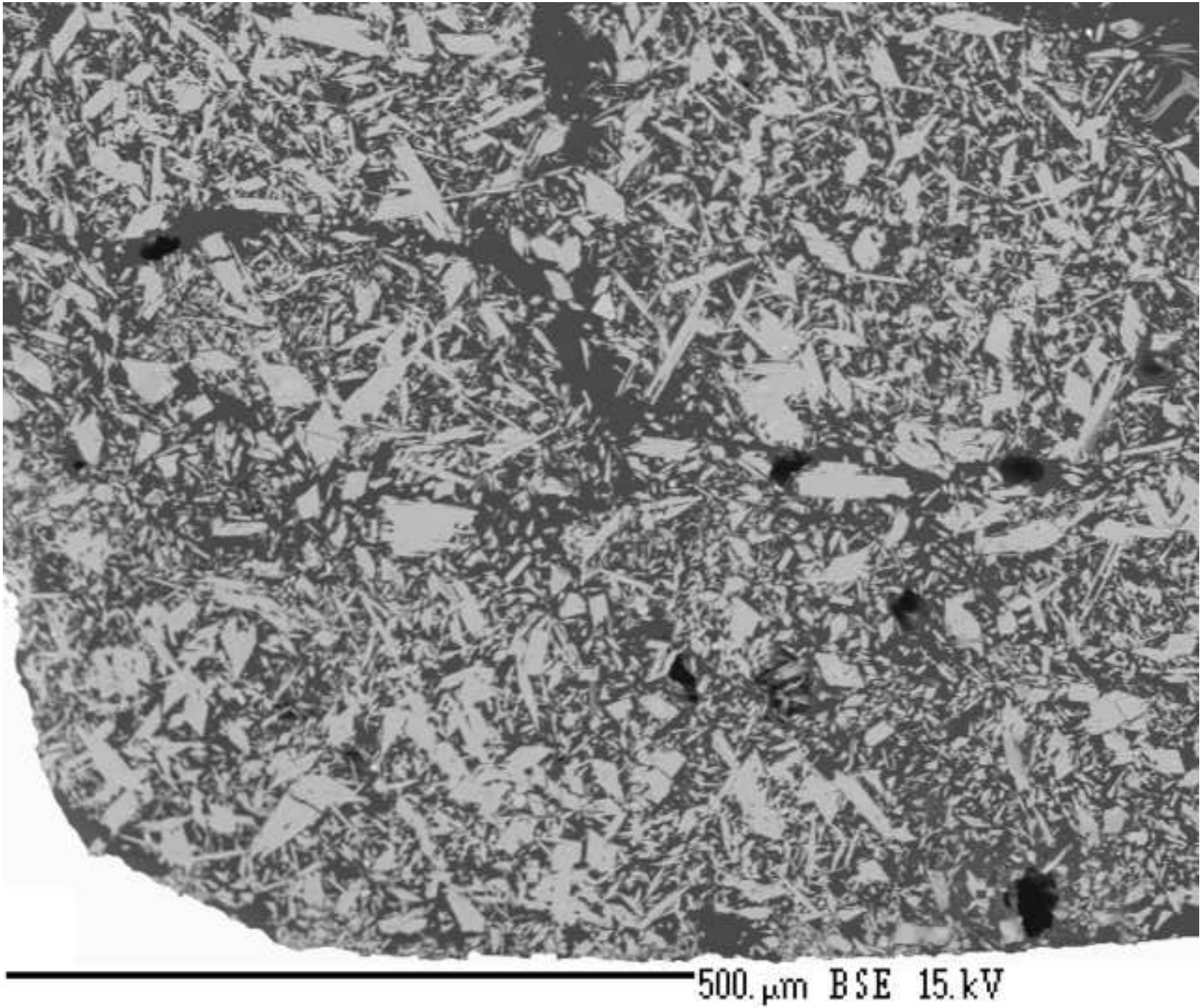

Figure 2c
Click here to download high resolution image

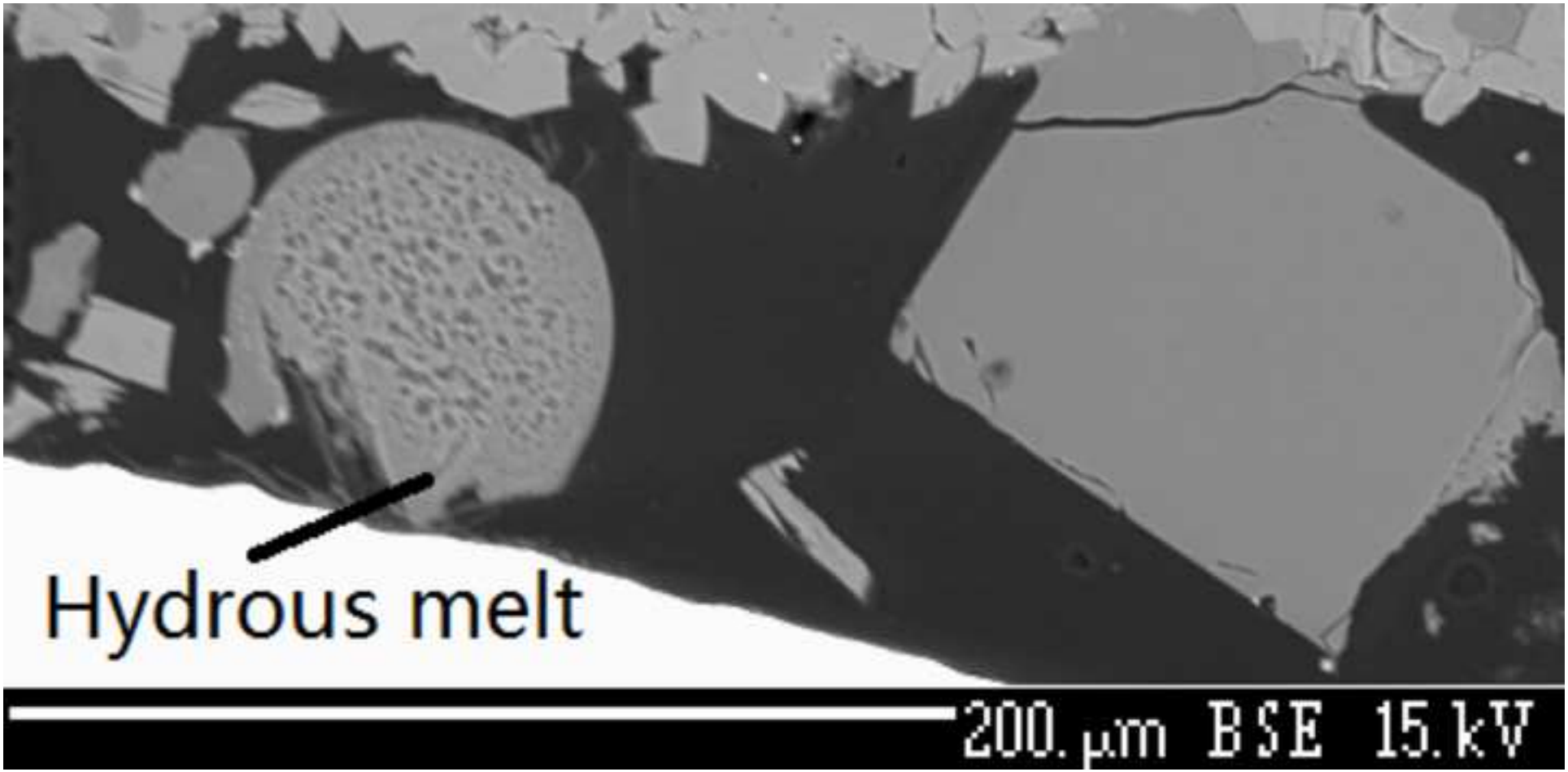

Figure 2d
Click here to download high resolution image

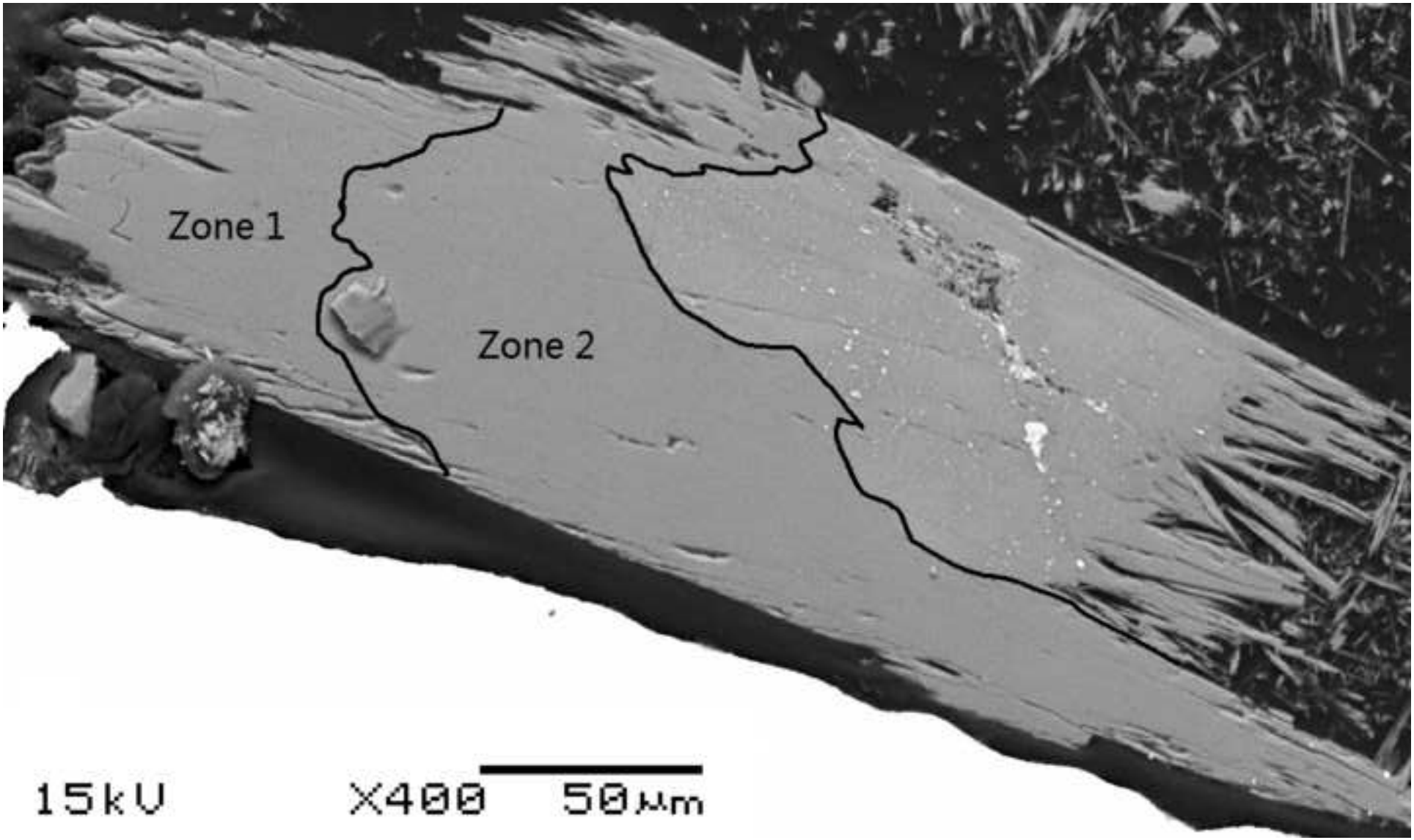

Figure 3

Click here to download high resolution image

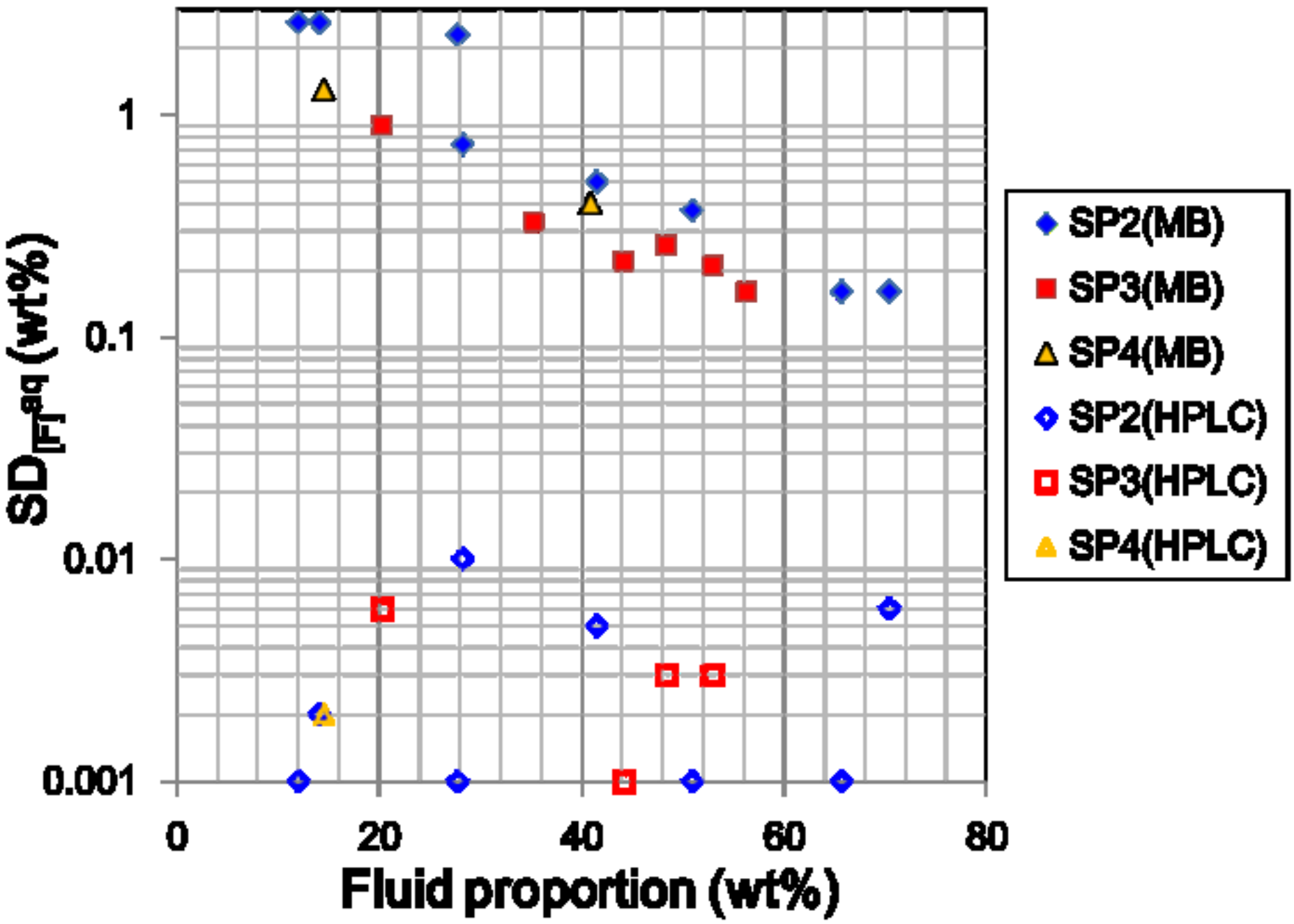

Figure 4a

Click here to download high resolution image

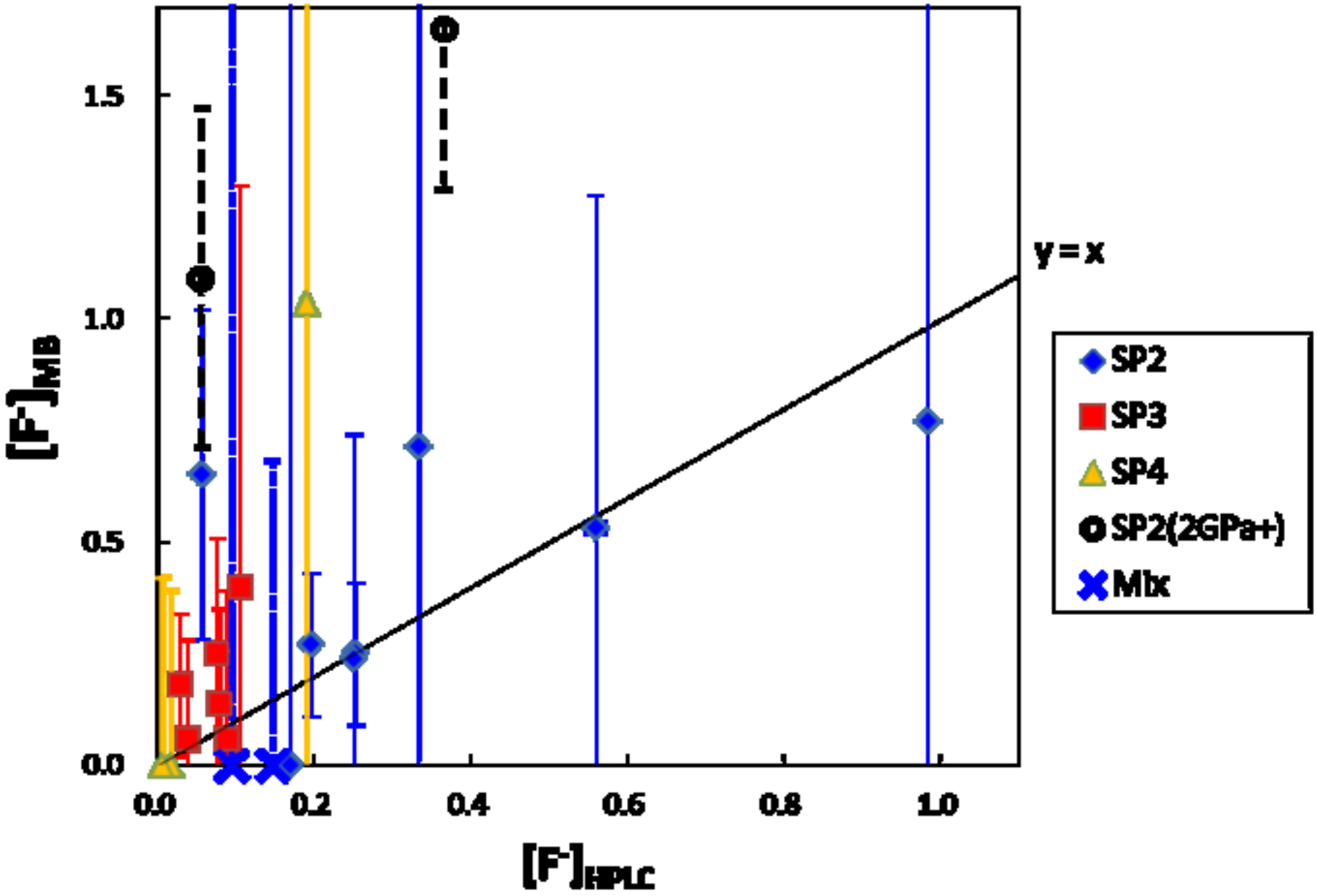

Figure 4b

Click here to download high resolution image

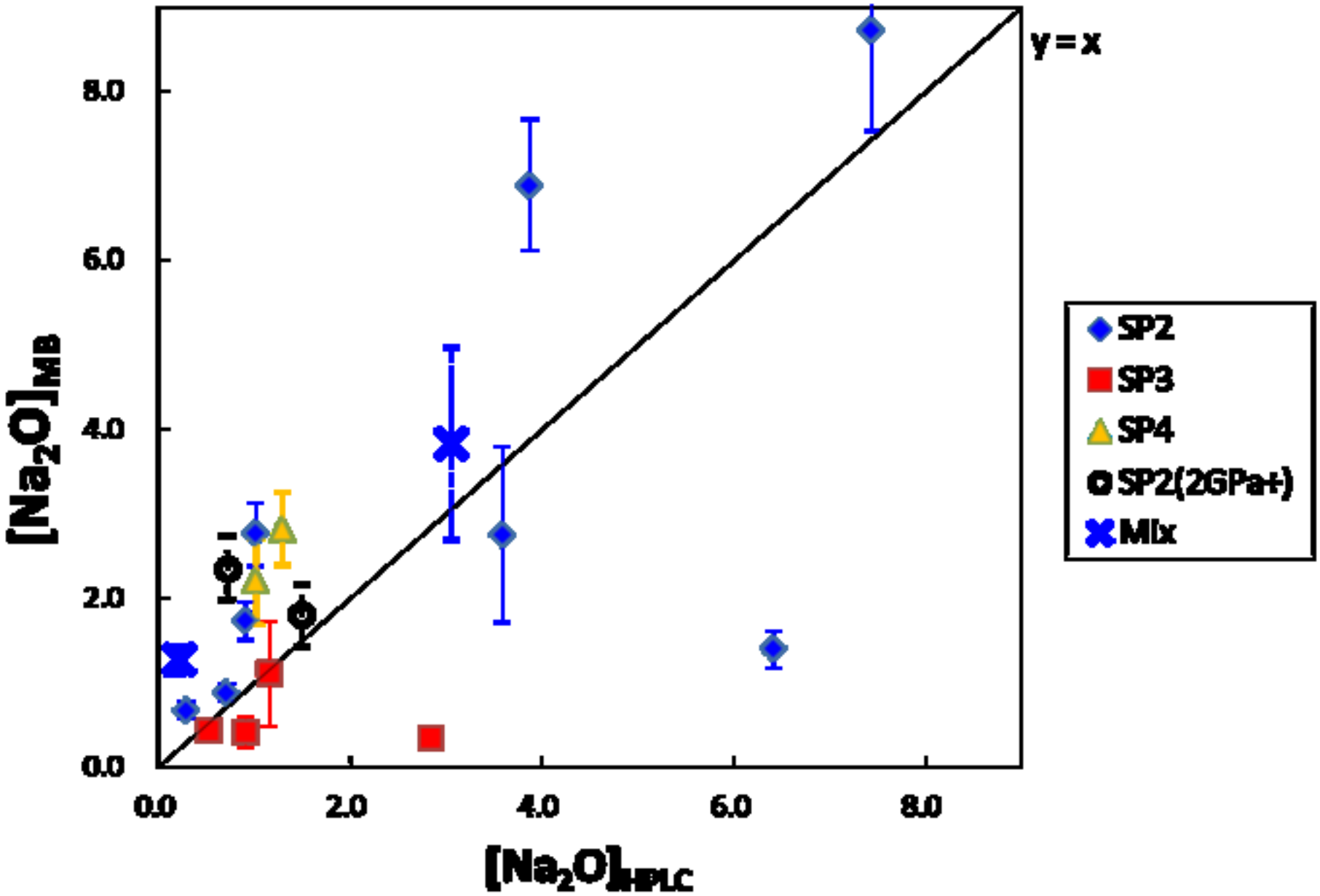

Figure 5
Click here to download high resolution image

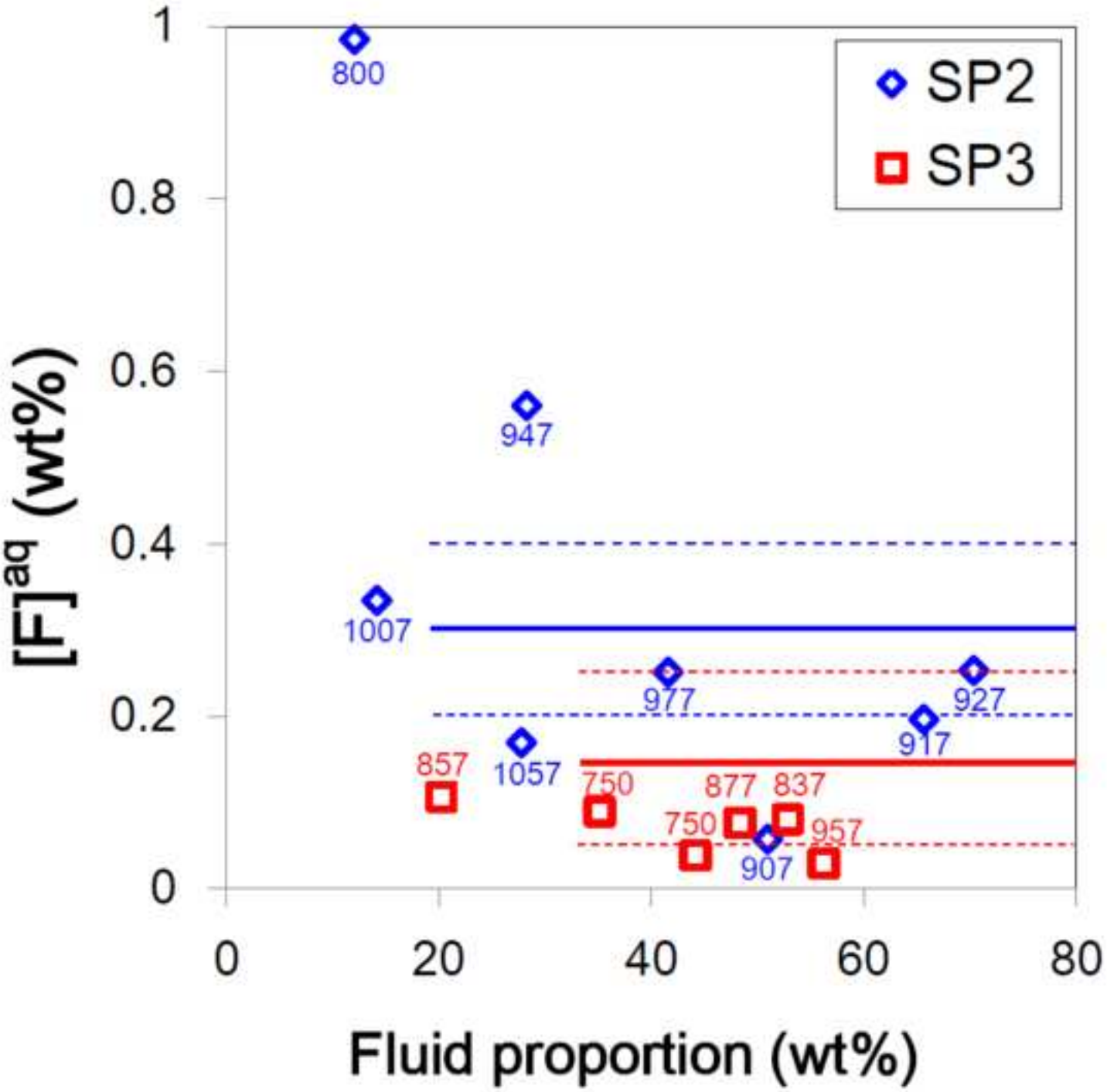

Table 1: Compositions of starting materials (unit: wt%)

	SP1	SP2	SP3	SP4	Richterite*
SiO_2	47.5(4)	43.1(6)	47.3(2)	37.5(1.0)	44.2(7)
TiO_2	0.42(6)	0.36(4)	0.38(3)	0.3(2)	4.3(3)
Al_2O_3	13.4(2)	12.1(2)	12.9(1)	10.1(5)	9.6(3)
Cr_2O_3	0.72(6)	0.67(8)	0.71(5)	0.6(2)	0.04(4)
FeO	3.6(1)	3.1(2)	3.57(8)	2.9(4)	10.9(4)
MgO	20.4(1)	24.0(3)	20.4(2)	37.0(9)	13.8(4)
CaO	11.7(2)	10.6(2)	11.4(1)	9.0(6)	10.2(4)
MnO	0.09(4)	0.09(4)	0.07(3)	0.07(15)	0.05(9)
Na_2O	1.44(7)	2.1(1)	1.36(5)	2.1(3)	4.3(3)
F	0.02(2)	4.81(7)	1.88(5)	0.51(24)	n.d
Total	99.3	101.6	100.0	100.0	97.6

Uncertainties given in parentheses apply to the last digit cited. n.d indicates “not determined”.

*the seed mineral composition in 1-SP3-11.

Table 2

Click here to download Table: Table2(V2.2).docx

Table 2: Experimental conditions, product proportions, and fluorine concentrations from mass balance calculations and HPLC measurements

Expt. ID	Conditions		Starting material		Fluid (mg)	Diluted factor	Phase assemblies (wt%)	F concentrations (wt%)		D_F(Flu/Hbl)	
	T (ºC)	Duration (h)	Solid (mg)	H_2O (mg)				MB	HPLC	MB	HPLC
1-SP1-8	807	114	1.91(1)	2.96(4)	1.21(4)	8074	Hbl(61.2), Flu(38.8)	n.d.	n.d.	n.d.	n.d.
1-SP2-24	750	215	3.27(1)	5.9(1)	0.71(1)	34401	Hbl, Nrb, Flu	n.d.	0.295(1)	n.d.	n.d.
1-SP2-23	800	143	4.78(2)	5.3(1)	0.45(1)	54278	Hbl(73.8), Nrb(14.1), Flu(12.1)	0.8(2.6)	0.985(1)	0.06(97)	0.416(64)
1-SP2-14	877	120	1.5(1)	2.6(1)	0.6(1)	16283	Hbl, Nrb, Chn, Flu	n.d.	0.082(1)	n.d.	0.040(5)
1-SP2-15	907	91	1.4(1)	2.2(1)	1.27(8)	26925	Hbl(40.6), Nrb(8.5), Flu(51.0)	0.65(37)	0.057(1)	0.29(17)	***0.026(3)***[b]
1-SP2-17	917	100	1.64(5)	3.3(1)	2.66(3)	3673	Hbl(27.6), Nrb(6.7), Flu(65.7)	0.27(16)	0.196(1)	0.13(8)	***0.093(12)***[b]
1-SP2-16	927	34	1.31(8)	3.65(5)	2.77(5)	17635	Hbl(23.9), Nrb(5.8), Flu(70.4)	0.25(16)	0.253(6)	0.11(8)	***0.114(14)***[b]
1-SP2-18	947	117	1.80(2)	2.03(2)	0.73(1)	13384	Hbl(52.6), Nrb(10.5), Melt(4.3), Precipitate(4.3), Flu(28.3)	0.53(74)	0.56(1)	0.32(25)	***0.251(37)***[b]
1-SP2-19	977	94	1.35(2)	n.d.	1.00(4)	9770	Hbl(25.5), Chn(11.6), Melt(21.3), Flu(41.6)	0.24(50)	0.251(5)	0.23(12)	***0.121(10)***[b]
1-SP2-20	1007	74	1.53(3)	3.05(1)	0.30(1)	32567	Hbl(32.6), Chn(19.2), Spl(0.7), Melt(33.3), Flu(14.2)	0.7(2.6)	0.334(2)	0.35(1.30)	0.166(18)
1-SP2-21	1057	73	1.86(2)	1.38(5)	0.84(1)	11631	Hu(15.4), Spl(1.2), Melt(55.6), Flu(27.8)	0.0(2.3)	0.169(1)	n.d.	n.d.
3-SP2-1	877	96	1.44(3)	5.15(3)	0.94(3)	10394	Hbl(47.4), Nrb(10.4), Flu(42.3)	1.65(36)	0.365(2)	1.03(27)	0.227(24)
4-SP2-2	877	191	2.04(3)	n.d.	1.62(6)	6031	OH-Grs(29.4), Nrb(13.4), Aug(7.5), Flu(49.7)	1.09(38)	0.055(1)	n.d.	n.d.
1-SP3-10[a]	750	135	1.89(2)	8.24(2)	1.34(1)	7440	Hbl(51.1), Chn(4.8), Flu(44.2)	0.06(22)	0.038(1)	0.04(16)	***0.027(4)***[b]
1-SP3-11[a]	750	141	2.60(1)	11.5(1)	1.16(1)	42974	Hbl(59.0), Chn(5.8), Flu(35.2)	0.06(33)	0.089	0.04(23)	***0.063(8)***[b]
1-SP3-4	837	169	1.7(1)	2.3(1)	1.76(4)	11102	Hbl(44.2), Chn(2.9), Flu(52.9)	0.14(21)	0.080(3)	0.10(15)	***0.056(9)***[b]
1-SP3-3	857	119	1.4(1)	1.7(1)	0.28(5)	34893	Hbl(74.8), Chn(5.0), Flu(20.3)	0.40(90)	0.106(6)	0.27(61)	0.071(11)
1-SP3-1	877	160	1.3(1)	2.1(1)	1.09(5)	8963	Hbl(48.6), Chn(3.0), Flu(48.4)	0.25(26)	0.076(3)	0.18(19)	***0.054(9)***[b]
1-SP3-8	957	96	1.64(4)	2.34(6)	1.91(2)	5115	Hbl(41.0), Chn(2.7), Flu(56.3)	0.18(16)	0.029	0.12(11)	***0.020(3)***[b]
1-SP4-4	843	143	1.50(2)	2.59(2)	0.85(2)	11494	Hbl(10.9), Aug(15.9), Chu(32.4), Flu(40.8)	0.0(4)	0.006	0.0(7)	0.011(3)

Expt. ID	Conditions		Starting material		Fluid (mg)	Diluted factor	Phase assemblies (wt%)	F concentrations (wt%)		D_F(Flu/Hbl)	
	T (ºC)	Duration (h)	Solid (mg)	H_2O (mg)				MB	HPLC	MB	HPLC
1-SP4-3	890	>68	2.13(3)	3.03(5)	1.43(1)	6832	Cln(15.2), Aug(14.0), Chu(30.0), Flu(40.9)	0.0(4)	0.017	n.d.	n.d.
1-SP4-5	950	127	2.51(1)	9.6(1)	0.40(1)	24425	Cln(21.2), Aug(19.0), Ol(45.1), Flu(14.6)	1.0(1.3)	0.190(2)	n.d.	n.d.
1-(SP2 + Qtz)	950	94	4.28(1) [SP2] + 6.63(1) [Qtz]	6.1(1)	4.53(1)	2157	Hbl(10.0), Talc(19.8), Melt(40.8), Flu(29.3)	0.0(7)	0.147(1)	0.00(31)	0.066(11)
1-(SP1 + MgF_2)	965	118	6.37(2) [SP1] + 0.77(1) [MgF_2]	8.2(1)	1.25(2)	19540	Chn(25.0), Spl(2.2), Melt(59.7), Flu(13.1)	0.0(8.4)	0.095(2)	n.d.	n.d.

The first numbers of Expt. ID indicate the experimental pressure during annealing: 1, 3, and 4 represents 1.0, 2.0, and 2.5 GPa, respectively.

Concentrations are in wt%. For mass balance results, 2σ errors are reported in parentheses; HPLC analyses generally conducted twice, the errors represent the difference between the results and the average value; The data without uncertainties indicates that the measurement only performed once. Uncertainties given in parentheses apply to the last digit cited.

n.d indicates “not determined”. Abbreviations, Hbl : hornblende ; Nrb : norbergite ; Chn : chondrodite ; Hu : humite; Chu : clinohumite; OH-Grs : hydrogrossular; Cln : clintonite; Aug: augite; Ol:olivine; Spl: spinel; Flu: fluid.

Phase proportions are calculated by mass-balance approach. Uncertainties given in parentheses apply to the last digit cited.

[a] The phase proportions are calculated with the chondrodite composition from 1-SP3-3, for SP3 experiments are in equilibrium in the Hbl-Chn-Flu system.

[b] The values of D_F(Flu/Hbl) in ***bond italic fonts*** from HPLC measurements indicates that the fluid proportion of experiments from SP2 and SP3 groups are higher than 30 wt%.

Table 3
Click here to download Table: Table3(V1.1).docx

Table 3 Relative complexed fluorine concentrations in 1-SP2-16 extracted solution

Ions	Concentration		lgK_1	lgK_2	lgK_3	relative
	ppb	10^{-9} mol/L				$[F^-]_{complexed}$ (%)
F^-	142	7470				
Fe^{3+}	0.264	4.74	5.28	9.30	12.06	0.04
Al^{3+}	4.74	87.8	6.10	11.15	15.00	0.2
Mg^{2+}	0.618	25.4	1.30			$<10^{-5}$

The cumulative formation constants are derived from Lange's handbook of chemistry.

appendix

Click here to download Table: Appendix (V3.1).docx

Appendix: Compositions of solid phases

Expt. ID	T/°C	Phases	Na_2O	K_2O	FeO	MgO	CaO	MnO	NiO	TiO_2	SiO_2	Al_2O_3	Cr_2O_3	F	H_2O	Total
1-SP2-23	800	Hbl	1.21(15)	0.03(5)	3.33(25)	19.03(45)	13.39(44)	0.10(8)	0.18(13)	0.43(8)	47.16(81)	11.43(96)	1.03(23)	2.37(37)	1.02(12)	99.69
		Nrb	0.01(5)	0.01(5)	3.10(79)	56.31(97)	0.53(11)	0.17(10)	0.25(21)	0.61(15)	27.85(72)	0.15(11)	0.10(11)	18.1(1.0)	0.11(20)	107.20
1-SP2-18	947	Hbl	1.30(14)	0.03(5)	4.31(30)	18.96(41)	13.44(45)	0.06(9)	n.d.	0.23(11)	43.58(69)	13.30(33)	0.92(16)	2.22(33)	1.07(5)	98.36
		Nrb	0.02(5)	0.00(5)	0.71(13)	57.63(77)	0.23(8)	0.05(8)	n.d.	0.92(15)	29.10(54)	0.03(5)	0.10(9)	15.44(78)	1.47(16)	104.25
		Melt	0.63(21)	0.41(19)	1.61(37)	13.75(99)	6.42(74)	0.06(19)	0.01(15)	0.45(25)	44.5(1.2)	19.32(84)	0.04(21)	6.4(1.2)	9.05(247)	102.71
		Precipitate	0.45(19)	0.05(12)	0.97(30)	9.86(85)	1.56(22)	0.09(17)	0.04(14)	0.22(22)	53.4(1.3)	18.04(68)	0.07(19)	4.6(1.0)	12.61	101.92
1-SP2-19	977	Hbl	1.42(15)	0.02(5)	4.21(28)	19.40(44)	13.54(50)	0.05(9)	0.08(11)	0.20(11)	43.79(82)	12.37(34)	0.97(16)	2.07(16)	1.14(2)	98.13
		Chn	0.00(5)	0.00(5)	1.19(16)	56.56(85)	0.16(7)	0.08(9)	0.13(11)	0.49(12)	34.77(70)	0.03(5)	0.08(10)	7.99(29)	1.41(9)	101.48
		Melt	0.66(16)	0.15(9)	2.63(34)	10.91(47)	13.37(68)	0.06(15)	0.02(11)	0.55(14)	44.4(1.0)	17.42(52)	0.02(16)	5.67(86)	6.51(71)	102.39
1-SP2-20	1007	Hbl	1.07(13)	0.01(5)	4.28(28)	19.26(39)	14.48(48)	0.06(9)	0.12(8)	0.22(11)	43.30(67)	13.40(40)	0.71(15)	2.02(22)	1.20(5)	98.92
		Chn	0.01(5)	0.01(5)	2.19(20)	55.98(64)	0.17(8)	0.11(9)	0.32(8)	0.57(13)	34.76(60)	0.04(5)	0.09(10)	7.51(39)	1.65(9)	101.76
		Spl	0.02(7)	0.01(5)	30.2(1.7)	17.96(41)	0.19(8)	0.28(12)	1.06(12)	0.21(10)	0.08(6)	26.7(1.4)	18.81(57)	n.d.	n.d.	95.55
		Melt1	1.01(26)	0.10(9)	2.99(36)	9.4(1.6)	13.76(70)	0.08(14)	0.03(11)	0.48(13)	41.0(1.3)	17.01(56)	0.05(16)	6.3(1.4)	10.4(3.7)	102.67
		Melt2	1.39(23)	0.10(11)	0.16(16)	0.17(9)	1.93(29)	0.02(13)	0.01(6)	0.04(11)	84.5(1.6)	7.19(34)	0.04(17)	0.88(40)	3.9(1.3)	100.37
1-SP2-21	1057	Hu	0.01(5)	0.01(5)	0.93(14)	56.09(83)	0.13(7)	0.05(8)	0.32(12)	0.31(11)	36.81(64)	0.03(5)	0.16(11)	5.14(36)	1.23(4)	99.98
		Spl	0.01(7)	0.00(6)	24.01(97)	20.48(48)	0.02(6)	0.20(11)	0.71(15)	0.17(10)	0.26(21)	14.63(35)	33.0(1.6)	n.d.	n.d.	93.49
		Melt	1.28(50)	0.12(15)	3.14(52)	13.8(1.1)	12.17(64)	0.11(19)	0.05(16)	0.29(24)	43.0(1.7)	13.80(66)	0.07(24)	5.1(1.1)	9.2(1.6)	102.15
3-SP2-1	877	Hbl	1.11(13)	0.01(5)	3.84(27)	18.23(39)	13.40(48)	0.09(9)	0.59(13)	0.17(10)	44.97(70)	13.39(31)	0.79(15)	1.61(24)	1.37(5)	98.18
		Nrb	0.01(5)	0.01(5)	1.64(18)	56.72(72)	0.19(7)	0.06(8)	0.65(13)	1.07(15)	29.06(54)	0.03(5)	0.06(10)	13.89(61)	2.20(11)	103.39
4-SP2-2	877	OH-Grs	0.01(5)	0.00(2)	5.62(74)	15.3(1.9)	13.9(1.9)	0.19(19)	n.d.	0.19(8)	39.7(1.2)	22.21(40)	1.08(37)	1.19(52)	0.73(41)	99.41
		Nrb	0.01(5)	0.00(2)	1.57(19)	55.82(86)	0.11(3)	0.01(14)	1.51(13)	1.17(7)	28.99(57)	0.04(5)	0.1(4)	13.24(55)	2.46(19)	102.58
		Aug	0.18(7)	0.01(5)	2.1(2)	16.35(41)	23.91(59)	0.04(9)	0.84(11)	0.06(7)	53.27(88)	2.53(18)	0.43(14)	0.09(12)	n.d.	99.81
1-SP3-10	750	Hbl	0.86(16)	0.02(5)	5.20(74)	17.07(69)	13.05(45)	0.10(9)	0.04(10)	0.63(14)	44.8(1.6)	13.7(2.9)	0.19(11)	1.39(18)	1.45(3)	97.06
		Chn [a]	0.00(5)	0.00(5)	0.98(15)	56.34(68)	0.06(6)	0.06(9)	0.60(10)	1.14(16)	34.46(59)	0.03(5)	0.06(10)	7.52(44)	1.63(7)	101.26
1-SP3-11	750	Hbl (zone1)	1.06(14)	0.01(5)	3.99(27)	18.33(40)	13.46(46)	0.09(9)	0.10(11)	0.57(13)	46.18(60)	12.07(97)	0.36(14)	1.42(18)	1.45(5)	97.65
		Hbl (zone2)	0.69(11)	0.00(5)	4.20(28)	16.30(38)	14.39(47)	0.07(9)	0.25(12)	0.81(15)	41.37(57)	17.83(35)	0.03(10)	1.82(21)	1.27(4)	97.76

Expt. ID	T/°C	Phases	Na_2O	K_2O	FeO	MgO	CaO	MnO	NiO	TiO_2	SiO_2	Al_2O_3	Cr_2O_3	F	H_2O	Total
		Chn [a]	0.00(5)	0.00(5)	0.98(15)	56.34(68)	0.06(6)	0.06(9)	0.6(1)	1.14(16)	34.46(59)	0.03(5)	0.06(10)	7.52(44)	1.63(7)	101.26
1-SP3-8	957	Hbl	0.92(12)	0.01(5)	3.86(29)	19.26(73)	12.95(45)	0.11(9)	0.07(8)	0.43(12)	44.0(1.6)	14.2(2.3)	0.37(27)	1.44(20)	1.41(6)	97.55
		Chn	0.02(5)	0.01(5)	1.21(18)	55.6(1.1)	0.32(44)	0.07(9)	0.19(8)	1.32(17)	35.0(6)	0.24(34)	0.08(10)	6.62(37)	2.09(4)	100.66
1-SP4-4	843	Hbl	3.16(22)	0.01(2)	4.46(30)	18.43(43)	13.40(22)	0.06(16)	n.d.	0.37(5)	40.63(79)	14.74(96)	0.41(5)	0.59(15)	1.80(4)	96.26
		Aug	0.36(51)	0.00(2)	2.94(34)	15.40(38)	24.1(1.6)	0.08(17)	n.d.	0.69(24)	49.0(1.0)	5.8(1.0)	0.90(26)	0.06(9)	n.d.	99.35
		Chu	0.00(4)	0.00(2)	0.88(16)	56.24(85)	0.22(3)	0.07(17)	n.d.	0.70(6)	38.16(68)	0.01(5)	0.02(4)	2.35(24)	1.75(1)	98.67
1-SP4-3	890	Cln	0.30(8)	0.00(2)	4.11(30)	20.99(45)	12.40(21)	0.00(16)	n.d.	0.15(4)	19.62(45)	34.47(52)	0.50(5)	0.58(14)	3.79(5)	93.14
		Aug	0.05(6)	0.00(2)	3.39(78)	14.84(74)	25.06(32)	0.05(16)	n.d.	0.57(23)	48.4(1.7)	5.9(1.5)	0.52(46)	0.07(9)	n.d.	98.83
		Chu	0.00(5)	0.00(2)	1.29(26)	55.36(84)	0.22(6)	0.09(17)	n.d.	0.74(6)	38.09(69)	0.04(5)	0.06(4)	2.32(24)	1.74(4)	98.21
1-SP4-5	950	Cln	0.01(3)	0.00(5)	3.25(24)	18.42(40)	12.80(45)	0.02(8)	5.43(48)	0.18(10)	18.95(41)	35.03(56)	0.29(12)	0.69(21)	3.75(2)	95.09
		Aug	0.01(5)	0.00(5)	2.8(5)	14.97(69)	25.86(66)	0.03(8)	0.80(11)	0.55(13)	48.3(1.5)	6.6(1.3)	0.20(12)	0.18(14)	n.d.	100.30
		Ol	0.00(5)	0.02(5)	0.36(11)	55.89(74)	0.29(9)	0.09(9)	1.48(33)	0.01(6)	42.45(66)	0.00(5)	0.00(6)	0.19(12)	n.d.	100.80
1-(SP2 +	950	Hbl	0.32(8)	0.01(5)	2.90(23)	22.35(50)	11.34(41)	0.03(9)	0.61(10)	0.44(8)	54.18(90)	4.63(18)	1.17(17)	2.21(35)	1.13(17)	100.20
Qtz)		Talc	0.03(6)	0.03(6)	0.69(13)	19.41(49)	0.05(6)	0.00(8)	16.67(40)	0.07(7)	58.58(98)	0.20(6)	0.21(12)	2.46(36)	3.22(18)	98.39
		Melt	0.35(11)	0.01(7)	0.64(19)	1.00(21)	4.26(36)	0.03(11)	0.16(11)	0.17(10)	76.9(1.4)	6.76(29)	0.05(14)	2.04(50)	8.51(74)	100.86
1-(SP1 +	965	Chn	0.01(5)	0.02(5)	2.54(25)	55.75(77)	0.19(7)	0.08(8)	0.51(13)	0.34(11)	33.77(53)	0.04(5)	0.14(11)	8.64(94)	1.04(17)	102.04
MgF_2)		Spl	0.01(7)	0.01(5)	27.7(3.3)	15.61(67)	0.57(44)	0.28(12)	1.68(28)	0.17(10)	0.39(65)	17.3(2.4)	31.5(3.0)	n.d.	n.d.	95.28
		Melt	0.91(26)	0.09(13)	2.74(48)	11.53(64)	14.83(95)	0.1(2)	0.08(22)	0.44(26)	38.5(1.1)	16.32(72)	0.02(23)	8.6(2.0)	9.45(153)	103.60

n.d indicates “not determined”. Abbreviations, Hbl : hornblende ; Nrb : norbergite ; Chn : chondrodite ; Hu : humite; Chu : clinohumite; OH-Grs : hydrogrossular; Cln : clintonite; Aug: augite; Ol:olivine; Spl: spinel.

Concentrations are in wt%, 2σ errors are reported in parentheses. Uncertainties given in parentheses apply to the last digit cited.

Water content is calculated by stoichiometry for minerals and charge balance for hydrous melt. Compositions of hydrous melt are normalized to 100%. “Total” values are did not exclude the oxygen substituted by F.

[a] Chn composition of 1-SP3-3 was used for 1-SP3-10 & 11 mass balance calculation. SP3 experiments are in equilibrium in the Hbl-Chn-Flu system.